The Aeronautical Journal (2024), **128**, pp. 2634–2655
doi:10.1017/aer.2024.52

ROYAL AERONAUTICAL SOCIETY

RESEARCH ARTICLE

Static and dynamic characteristics of supersonic cruise missile with damaged wing

C.F. Zhuo[1], Z.R. He[1], X.B. Ren[2] and Y.K. Wang[1]

[1]School of Mechanical Engineering, Key Laboratory of Special Engine Technology, Ministry of Education, Nanjing University of Science and Technology, Nanjing, China
[2]Shanxi North Xing'an Chemical Industry Co, Ltd, Taiyuan, China
Corresponding author: C.F. Zhuo; Email: njust203zcf@126.com

Received: 24 November 2023; **Revised:** 20 March 2024; **Accepted:** 24 April 2024

Keywords: supersonic cruise missile; wing damage; aerodynamic characteristics; combined dynamic derivative; damage limit

Abstract

Accurately evaluating the aerodynamic performance of the missile with damaged structures is very important for the subsequent flight control strategy. At present, few researchers have studied the aerodynamic characteristics of damaged supersonic cruise missiles. Based on CFD (computational fluid dynamics) solutions and the dynamic derivative identification method, the differences in static and dynamic characteristics between the damaged and undamaged models are compared. The results indicate that when the extent of damage increases, the change rate of drag coefficient at larger AoA (angle-of-attack) is greater than that at the smaller AoA. On the contrary, the change rate of lift coefficient at larger AoA is smaller than that at smaller AoA. Meanwhile, the absolute value of the static pitch moment decreases, but the absolute value of the roll moment increases. Damage causes a change in the absolute values of the pitch and roll dynamic derivatives, and the dynamic derivatives do not vary monotonically with the increase of AoA. The turning point occurs at about $\alpha = 5°$. The areas of the hysteresis loops of the pitch-roll coupling moment increase, which makes the dynamic coupling characteristic between the pitch and roll directions increase. Finally, the maximum allowable damage extent of the missile wing that can achieve static trim is obtained and validated by controlling the deflection of the four rudders.

Nomenclature

$C_{m\dot{\alpha}} + C_{mq}$	combined dynamic derivatives
C_d	coefficient of drag
C_l	coefficient of lift
C_{mx}	coefficient of roll moment
C_{my}	coefficient of pitch moment
h	wing damage width (m)
k	reduced frequency
l	maximum wing width (m)
Ma	Mach number
ω	oscillation frequency (rad/s)

1.0 Introduction

The rapid and continuous development of aerospace technology has a revolutionary impact on modern warfare. At present, tactical missiles should have the combat characteristics of multi-trajectories, long-range, high precision and strong penetration ability. Therefore, supersonic cruise missile has become one of the research hot spots in various countries, due to it can meet the above requirements. The increasingly

complex battlefield environment tests the viability of various missiles, and it is very important that the missiles can fly to a predetermined location [1, 2]. These missiles may have various combat damage modes during flight. For example, the fuel explosion leads to the disintegration of the missile, and the missile is hit by several interceptors or debris flying in the air and thus disintegrates [3]. These kinds of damage are irreparable. However, if only some parts of the missile structures are attacked and damaged, the control system may still use other undamaged parts to keep the flight [4]. In this case, it is significant to accurately evaluate the aerodynamic performance, because it directly determines the further flight ability and influences the next control strategy [5, 6].

Different interception methods will cause different types and extents of damage to the missile wings. Series of computational analyses and experiments of battle damage configurations have been carried out to evaluate the aerodynamic characteristics. At present, there are few works directly related to missile structural damage. Therefore, the studies of aircraft wing structure damage, which is similar to missile wing damage, also have a certain reference value. Aerodynamic simulation of damaged effects had been conducted to provide an understanding of the control and stability of aircraft with asymmetric damage by Elkarim and Elrahman [7]. A mathematical model and guidance algorithms were developed for an anti-tank missile by Harris and Slegers [8]. Monte Carlo simulations were performed for each type and location of the damaged mid-body wing. The results indicated that the damage response performance of the missile was extremely sensitive to the radial location of the damage. Irwin and Render [9] carried out wind tunnel tests on wings to simulate battle damage. Application of gunfire and missile fragmentation effects to solid and hollow wing models were implemented. The detrimental effects of these damages were greater for wings of solid construction. Djellal and Ouibrahim [10] evaluated the impact of wing shooting damage on the performance of typical aircraft models through two experimental studies, as well as how to repair the damage. The results showed the damage caused significant aerodynamic coefficient reduction related to the diameter and location of the holes. Patch repairs can achieve substantial recovery of the aerodynamic losses. Wen et al. [11] analysed the aerodynamic characteristics of an aircraft with structural damage by using trim, linearisation, stick-fixed response and disturbance simulation. The results indicated that the damage caused an offset to the centre of gravity and pitch-roll, pitch-yaw coupling. The remaining flight performance was studied by inducing the Remaining Capability Factor. Etemadi et al. [12] used CFD and experimental methods to evaluate the aerodynamic characteristics of damaged triangular and star-shaped aerofoils after repair. The results revealed the influence mechanism of structural damage on aircraft aerodynamic force and moment, and demonstrated the importance of shape factor in evaluating the performance. Nonlinear static aeroelastic behaviour of the damaged composite missile fins was investigated by Zkaya and Kayran [13]. Considering the generation of different damages, two-way coupled fluid-structure interaction (FSI) was carried out to predict the influence of the damage modes on the pressure distribution, lift and deformation of the damaged fin, and compared with that of the undamaged missile fin. A CFD study was carried out on a battle-damaged NACA 64_1-412 half wing by Yang et al. [14]. The previous experimental findings were confirmed. The flow field destroyed by simulated gunfire is asymmetric, and this asymmetry was driven by the spanwise variation of static pressure.

The selection of a set of feasible trim points becomes very important for controlling the aircraft under the influence of unfavourable conditions and failures. Continuation methods and bifurcation analyses were employed to determine the family of feasible level flight trim points of a military aircraft by Shankar [15]. Elgersma and Morton [16] presented closed-form formulas for computing all possible trim values for six-degree-of-freedom nonlinear aircraft models. The four-dimensional trim set was parameterised by giving at most two real trim values for each set of fixed values. A wind tunnel investigation was conducted to measure the aerodynamic effects of damage to lifting and stability/control surfaces of a commercial transport aircraft by Shah [17]. The author developed flight control systems to recover the aircraft from adverse, damage-related loss of control events and estimated aerodynamic characteristics from flight data.

These studies had further improved the practicability of studying performance on damaged missiles and aircrafts, but there is little research on wing damage of supersonic cruise missiles. Previous studies

https://doi.org/10.1017/aer.2024.52 Published online by Cambridge University Press

have showed that the aerodynamic performance of a missile with different types and extents of damage varies greatly. Generally, there are three categories of battle damage to missiles caused by interceptors: fragment, discrete rod and continuous rod damage. The former two have similar effects. Their typical performance is the perforation of missile parts. By comparison, continuous rod damage has a greater killing range and is always able to cut the missile into multiple parts. Considering the small impact of perforation damage on the wing, only one typical continuous rod damage [18] effect is analysed in this study. Meanwhile, the most important task for the damaged missile is how to control its flight by using the remaining rudder surfaces and the engine power [19]. Therefore, to optimise the flight control strategy, it is necessary to accurately calculate the aerodynamic performance of the damaged missile. The main contents of this study are as follows. First, the feasibility of the Spalart-Allmaras turbulence model in calculating the static and dynamic aerodynamic characteristics of the missile is validated. Then the aerodynamic characteristics of a simplified missile model after its right wing being damaged to different extents are calculated and compared. The changing rules and reasons are found. After that, the research on the dynamic pitch, roll and pitch-roll coupling characteristics of the damaged missile is emphasised. Finally, the maximum allowable damage extent of the missile wing that can achieve static trim is obtained when the maximum flight angle-of-attack is $\alpha = 12^\circ$ and the maximum deflection angle of the single rudder is $\beta = 15^\circ$.

2.0 Battle-damaged model and computational grids

2.1 Model

Four extents of the right wing damage are considered. The extent of damage is indicated by the missing wing span length. The maximum damage to the wing is 50%, which represents the worst-case damage reproducible during environmental drops performed by the Close Combat Weapons Systems Project Office and the US Marine Corp [20]. These parameters may not be consistent with the actual damaged situations, but they help to obtain the relationship between the change of aerodynamic performance and the damage extent of missile wing.

The model used in this study is a simplified version of a typical supersonic cruise missile. In order to conveniently make a comparison before and after damage, the axisymmetric inlet and aerofoil of the model are simplified, and the case of one wing damage is discussed in this paper. The parameters of geometric model are shown in Fig. 1, and they are measured in millimeters. W represents the wing and R represents the rudder in Fig. 1(b). h represents the damaged width in Fig. 1(c).

The wing of the missile is thin and light, so the change in the centre of gravity can be neglected. The parameters of the missile are shown in Table 1. The reference area is the maximum cross-sectional area of the missile body, and the reference length is the diameter of the missile. The moment reference point (MRP) is 2.5m from the missile head and it is also set as the point of rotation (POR) for dynamic simulation.

2.2 Mesh

The research adopts structured meshes. High-speed compressible flows involve important fluid phenomena typically exhibiting shock waves, rarefactions and related complexities [21]. Therefore, the mesh needs to be encrypted where the flow changes violently. For example, the mesh is encrypted when the geometric structure of the model changes. Figure 2 gives the computational mesh, including far field mesh and boundary layer mesh. The far-field length in the computational domain is 10 times the length and 20 times the diameter of the projectile.

Mesh independence is crucial to get the correct solution. An efficient mesh resolution must be determined to find correct calculation results and the appropriate amount of solution time [22]. The solution in this study is implemented by generating different mesh resolution between about 1.2 and 6.2 million. Figure 3 shows mesh independence for the drag coefficient (C_d) versus the number of mesh resolution.

https://doi.org/10.1017/aer.2024.52 Published online by Cambridge University Press

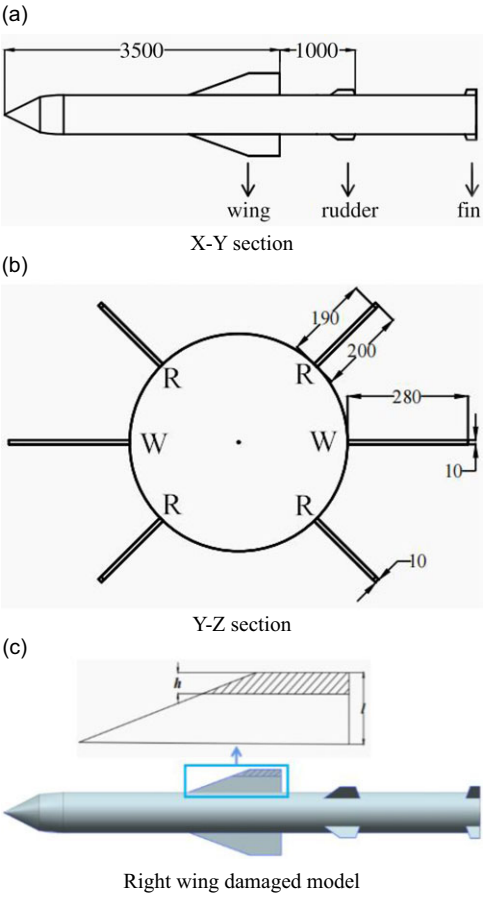

Figure 1. *Geometric model and damage diagram.*

The calculation result of 6.2 million mesh resolution is used as reference values. Table 2 shows that the change rate of C_d is all less than 2%. Since the solution results are negligible changes above 2.85 million mesh resolution, considering the calculation time cost, 2.85 million is chosen as the efficient mesh resolution.

3.0 Computational method

3.1 Fluid governing equation

The continuity equation and energy equation are referred to the Ref. [23]. The conservation form of the 3D dimensionless, unsteady, compressible, Reynolds-averaged Navier–Stokes equations in Cartesian coordinates is as follows [24]:

$$\frac{\partial \boldsymbol{Q}}{\partial t}+\frac{\partial \boldsymbol{F}}{\partial x}+\frac{\partial \boldsymbol{G}}{\partial y}+\frac{\partial \boldsymbol{H}}{\partial z}=\left[\frac{\partial \boldsymbol{F}_v}{\partial x}+\frac{\partial \boldsymbol{G}_v}{\partial y}+\frac{\partial \boldsymbol{H}_v}{\partial z}\right]$$

$$\boldsymbol{Q}=\begin{bmatrix}\rho\\ \rho u\\ \rho v\\ \rho w\\ \rho E\end{bmatrix},\boldsymbol{F}=\begin{bmatrix}\rho u\\ \rho u^2+p\\ \rho uv\\ \rho uw\\ \rho Hu\end{bmatrix},\boldsymbol{G}=\begin{bmatrix}\rho v\\ \rho uv\\ \rho v^2+p\\ \rho vw\\ \rho Hv\end{bmatrix}$$

https://doi.org/10.1017/aer.2024.52 Published online by Cambridge University Press

Table 1. *Basic parameters of missile*

Parameter	Value
Length	6m
Diameter	0.5m
Reference area	$0.19625m^2$
Reference length	0.5m
MRP and POR	$X = 2.5m$

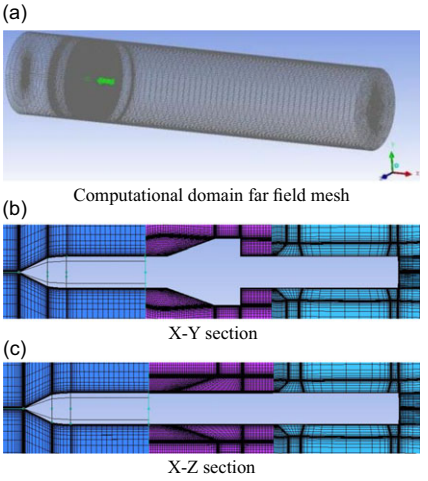

Figure 2. *Mesh generation of the missile.*

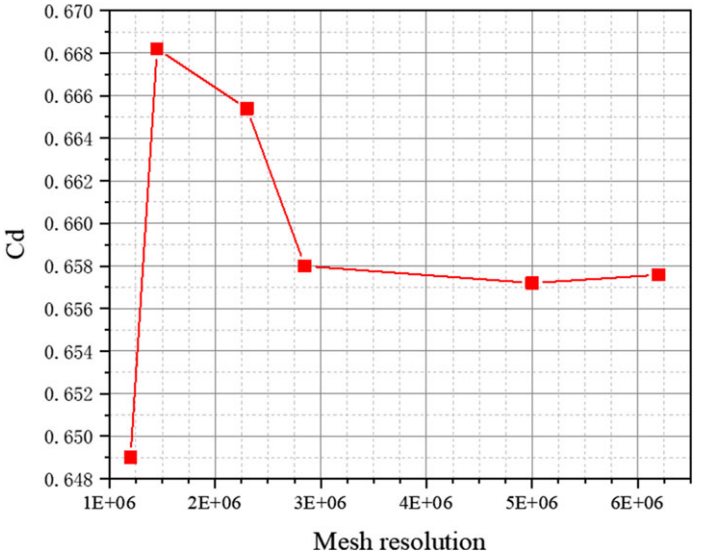

Figure 3. *Mesh independence validation.*

https://doi.org/10.1017/aer.2024.52 Published online by Cambridge University Press

Table 2. *Mesh independence error of Cd*

Mesh resolution (million)	Error (%)
1.2	1.3048
1.45	1.6150
2.3	1.1892
2.85	0.0639
5	0.0578

$$\boldsymbol{H}=\begin{bmatrix}\rho w\\ \rho uw\\ \rho vw\\ \rho w^2+p\\ \rho Hw\end{bmatrix},\boldsymbol{F}_v=\begin{bmatrix}0\\ \tau_{xx}\\ \tau_{xy}\\ \tau_{xz}\\ \tau_{xx}u+\tau_{xy}v+\tau_{xz}w+q_x\end{bmatrix} \tag{1}$$

$$\boldsymbol{G}_v=\begin{bmatrix}0\\ \tau_{yx}\\ \tau_{yy}\\ \tau_{yz}\\ \tau_{yx}u+\tau_{yy}v+\tau_{yz}w+q_y\end{bmatrix}$$

$$\boldsymbol{H}_v=\begin{bmatrix}0\\ \tau_{zx}\\ \tau_{xy}\\ \tau_{zz}\\ \tau_{xx}u+\tau_{zy}v+\tau_{zz}w+q_z\end{bmatrix}$$

where p is pressure, ρ is density, (u, v, w) are the Cartesian velocity components, $\boldsymbol{E}$ is total specific energy, $\boldsymbol{H}$ is total specific enthalpy, $H=E+p/\rho$, $\boldsymbol{Q}$ is the conserved variable, $\boldsymbol{F}, \boldsymbol{G}, \boldsymbol{H}$ are the convective terms, $\boldsymbol{F}_v$, $\boldsymbol{G}_v$ and $\boldsymbol{H}_v$ are the viscous terms.

3.2 Discrete scheme and solution method

The discrete scheme used in this study is Roe-FDS. The spatial discrete scheme is the second order upwind. The solution method is to adopt the density-based solution, velocity component and density are taken as basic variables, and the pressure is obtained by state equation. The density based solution is solved by coupling algorithm. The continuity equation, momentum equation and energy equation are solved simultaneously, and then other scalar equations are solved sequentially.

3.3 Turbulence model

Spalart-Allmaras (S-A) turbulence model is a simple single equation model for a modified turbulent kinematic viscosity [25]. It is specially designed for aerospace applications. And it has a good application in the calculation of missile external flow field [26]. Compared with the two-equation model, it has lower

https://doi.org/10.1017/aer.2024.52 Published online by Cambridge University Press

encryption requirements for the computing grid on the wall. And it has the advantage of good stability. Previous studies [27] on battle-damaged aerofoils had shown this model produced reasonable result, and outperformed the k-ε model slightly. The transport equation of the Spalart-Allmaras model is adopted as the governing equation, and its form can be obtained from the Refs [28, 29].

3.4 Boundary and initial conditions

Pressure-far-field condition is adopted at the entrance and radial boundary of the computational domain. Pressure-out condition is adopted at the outlet, the temperature and pressure are the same as the far-field. The surface of missile adopts non-slip solid wall boundary condition. The initial value of the computational flow field is set as the free flow value. The fluid types in the computational domain is ideal gas, and the viscosity is calculated using Sutherland's law.

3.5 Dynamic derivative identification method

Forced motion offers a good alternative to predict the aerodynamic coefficients of an aircraft [30]. The classic method for calculating dynamic derivatives is the small amplitude oscillation technique. It evolved from the wind tunnel tests and can calculate subsonic, transonic and supersonic states [31]. The Fourier expansion of unsteady aerodynamic moment on rigid aircraft with small amplitude forced pitch vibration is given as follows:

$$M_z = M_{z_0} + \bar{M}_z \sin(\omega t + \lambda) + u(t) \tag{2}$$

According to the concept of aerodynamic derivative, the unsteady aerodynamic moment of the rigid aircraft with small amplitude forced pitch vibration can be expressed by Taylor expansion as follows:

$$M_Z = M_{z_0} + M_z^{\alpha}\Delta\alpha + M_z^{\dot{\alpha}}\Delta\dot{\alpha} + M_z^{\omega_z}\omega_z + M_z^{\dot{\omega}_z}\dot{\omega}_z + \hat{\Delta}\,(\Delta\alpha, \omega_z) \tag{3}$$

Where, M_z is the transient unsteady aerodynamic moment; M_{z_0} is the aerodynamic moment at the equilibrium position. M_z^{α} is the static derivative of aerodynamic moment; $M_z^{\dot{\alpha}}$ is the first dynamic derivative of aerodynamic moment to AoA; $M_z^{\omega_z}$ is the zero-order dynamic derivative of aerodynamic moment to pitch angular velocity; $M_z^{\dot{\omega}_z}$ is the first dynamic derivative of aerodynamic moment to pitch angular velocity; $\hat{\Delta}$ is a higher-order derivative term. When the rigid aircraft oscillates in small amplitude, its motion equation can be simplified as:

$$\begin{cases} \theta = \theta_m \sin(\omega t) \\ \dot{\theta} = \omega\theta_m \cos(\omega t) = \omega_z \\ \ddot{\theta} = -\omega^2\theta_m \sin(\omega t) = \dot{\omega}_z \\ \Delta\alpha = \theta = \theta_m \sin(\omega t) \\ \Delta\dot{\alpha} = \dot{\theta} = \omega\theta_m \cos(\omega t) \end{cases} \tag{4}$$

Substituting Equation (4) into Equation (3) and omitting high-order component $\hat{\Delta}$:

$$\begin{aligned} M_Z = {} & (M_Z^{\alpha} - \omega^2 M_Z^{\dot{\omega}_Z})\theta_m \sin(\omega t) \\ & + (M_Z^{\dot{\alpha}} + M_Z^{\omega_Z})\omega\theta_m \cos(\omega t) + M_{Z_0} \end{aligned} \tag{5}$$

When the calculation time of the unsteady problem is long enough, the aerodynamic moment changes periodically, and the single point method can be adopted [32], making $\omega t = 2n\pi$ to remove the influence of the initial effect, so Equation (5) can be written as follows:

$$M_z^{\dot{\alpha}} + M_z^{\omega_z} = \frac{\bar{M}_z \sin\lambda}{\omega\theta_m} = \frac{M_{\omega t = 2n\pi} - M_{z_0}}{\omega\theta_m} \tag{6}$$

https://doi.org/10.1017/aer.2024.52 Published online by Cambridge University Press

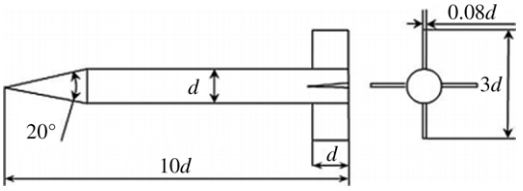

Figure 4. *Basic Finner missile model.*

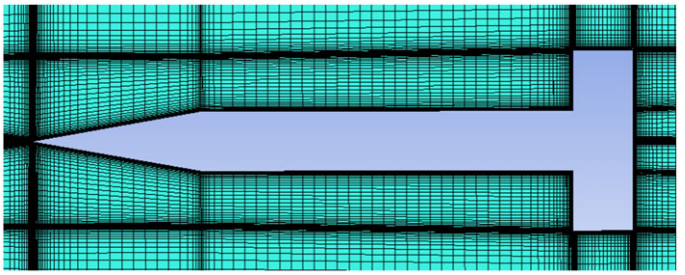

Figure 5. *Mesh generation of Basic Finner missile.*

Make dimensionless treatment on the above formula. The reduced frequency is $k = \omega l/2V_\infty$, where l is the reference length and V_∞ is the far-field free inflow velocity, substituting and obtaining:

$$C_{mq} + C_{m\dot{\alpha}} = \frac{M_{\omega t=2n\pi} - M_{z0}}{kqsl\theta_m} = \frac{C_{M_{\omega t=2n\pi}} - C_{M_{z0}}}{k\theta_m} \tag{7}$$

where $C_{M_{\omega t=2n\pi}}$ is the instantaneous pitching moment coefficient at $\omega t = 2n\pi$, and $C_{M_{z0}}$ is the steady moment coefficient at the equilibrium position. k is the reduced frequency, q is the dynamic pressure, s and l are the reference area and length respectively, and θ_m is the amplitude.

3.6 Method validation

The Basic Finner missile model is the international standard model to validate the aerodynamic calculation. The model of the missile is shown in Fig. 4. The structural parameters are consistent with those in Ref. [33], that is, $d = 30$mm.The computational mesh of the missile is shown in Fig. 5, and the number of grids is 2.6m. The length of the far field in the calculation domain is 10 times the length of the missile and the diameter is 20 times the diameter of the missile. The calculation conditions in this study are consistent with the Ref. [34], that is, Ma = 1.58, initial attack angle $\theta_0 = 0°$, frequency reduction rate $k = 0.0158226$, amplitude $\theta_m = 1°$, so the oscillation law can be written as $\alpha = \theta_0 + \theta_m \sin(\omega t) = 1°\sin(571.7t)$.

Experimental data was obtained from a combination of free-flight tests in a ballistic range and wind tunnel measurements at different test facilities [35, 36].

The hysteresis loops of pitch moment coefficient obtained from the calculation in this study is shown in Fig. 6. The curve basically coincides with the CFD calculation value in the Ref. [34], indicating that the error is small. The errors of $C_{m\dot{\alpha}} + C_{mq}$ are shown in Table 3. Error-C represents the error with the calculated value [37], and Error-E represents the error with the experimental value [33]. Compared with the experimental and calculated values, the error of the S-A model obtained in this study is larger, but it is still less than 8%. One aspect of the analysis that contributes to this error may be due to insufficient number of grids and insufficient precision of numerical methods. On the other hand, the edge of the numerical calculation model is sharp, but the test piece usually has a certain chamfer, not a completely

https://doi.org/10.1017/aer.2024.52 Published online by Cambridge University Press

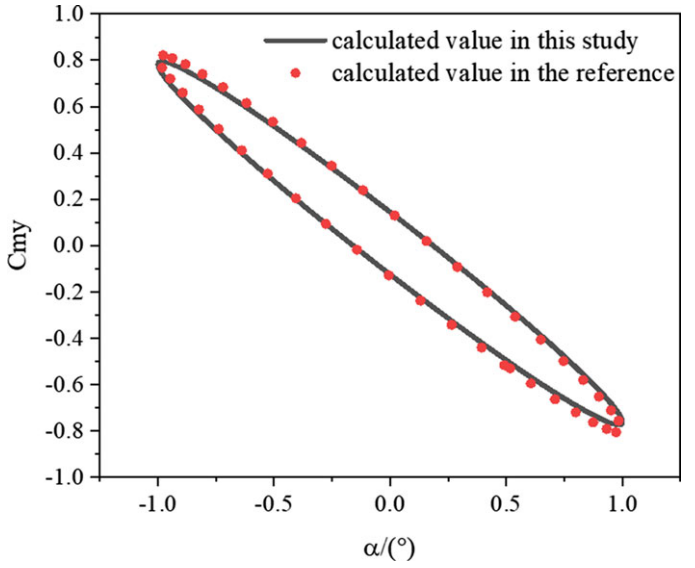

Figure 6. *Hysteresis loops of Cmy (Cmy represents the pitch moment coefficient).*

sharp edge, which may also cause errors between the numerical calculation and the test results. This error is acceptable, indicating that the calculation method has high reliability for calculating the aerodynamic characteristics of the missile model in this study.

4.0 Results and discussions

4.1 Static aerodynamic characteristics

First, the static aerodynamic characteristics of all models with different damage extent are simulated. The calculation conditions are listed in Table 4.

The differences before and after damage are analysed in terms of the flow field. Due to large number of calculation conditions and limited space, only some representative flow field contours of the damaged models are selected for display, i.e., the models with the right wing of $0.3l$ and $0.5l$ damage at $\alpha = 4°$ and $\alpha = 8°$.

Figures 7 and 8 show the Mach and local pressure contour around the models. The oblique shock waves formed in front of the head, wings, rudders and fins of the missile can be clearly seen in the figures. The low Mach number region at the tail of the missile is also obvious. By comparison, it is found that when the AoA changes from $\alpha = 4°$ to $\alpha = 8°$, a local high Mach number region appears behind the wing on the undamaged side (left side). On the side of the damaged wing, the region is small. When the damage extent reaches $0.5l$, the above phenomenon hardly appears, which makes the flow field on both sides of the missile asymmetric.

Figures 9 and 10 show the streamlines and vortices around the models. After being damaged, the flow field asymmetry becomes larger on both sides of the missile. This asymmetry is more obvious when the AoA increases. The vortices on both sides of the missile differs significantly. The vortices formed by the damaged wing are longer but smaller in diameter compared to the undamaged left side. The streamlines show that the vortices on the damaged side become more concentrated. Compared with the left wings, the vortices formed by the right wings of the two damaged models are closer to the body of the missile and extend to the rear side of the fin at $\alpha = 8°$, which affects the flow field around the rudders and fins behind the wings.

https://doi.org/10.1017/aer.2024.52 Published online by Cambridge University Press

Table 3. *$C_{m\dot{\alpha}} + C_{mq}$ comparison of Basic Finner missile*

Calculation in this study	Calculation in the reference	Experiment	Error-C	Error-E
−484.44	−506	−526	4.26%	7.90%

Table 4. *Static calculation conditions*

Parameter	Value
Mach number Ma	2.5
Cruising altitude H	0.1km
AoA α	0°, 4°, 8°, 12°

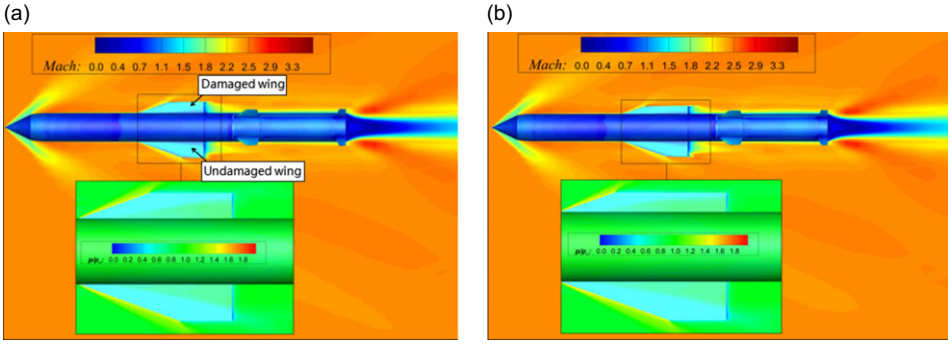

h/l=0.3 damaged model *h/l*=0.5 damaged model

Figure 7. *Mach and local pressure contour at $\alpha = 4°$.*

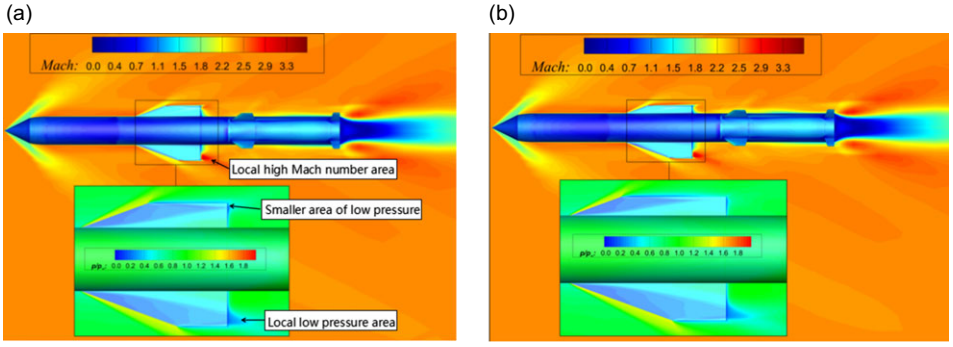

h/l=0.3 damaged model *h/l*=0.5 damaged model

Figure 8. *Mach and local pressure contour at $\alpha = 8°$.*

To further explore the effect of wing damage on the flow field around the missile, the pressure distribution around the wings, rudders and fins of the missile are shown separately to compare their differences (the missile body is hidden for better visibility). Due to the limitation of space, the representative pressure contour distribution at $\alpha = 8°$ is selected for display. As shown in Fig. 11, the wingtip vortices of the damaged wings are smaller than that of the undamaged wing and appear mainly in part of the wing parallel to the body. However, the pressure distribution at the leading edge of the wing is almost unaffected by the damage. As the damage extent increases, the wingtip vortices become smaller and the pressure gradient changes more drastically. This leads to a decrease in the lift coefficient and a non-linear

https://doi.org/10.1017/aer.2024.52 Published online by Cambridge University Press

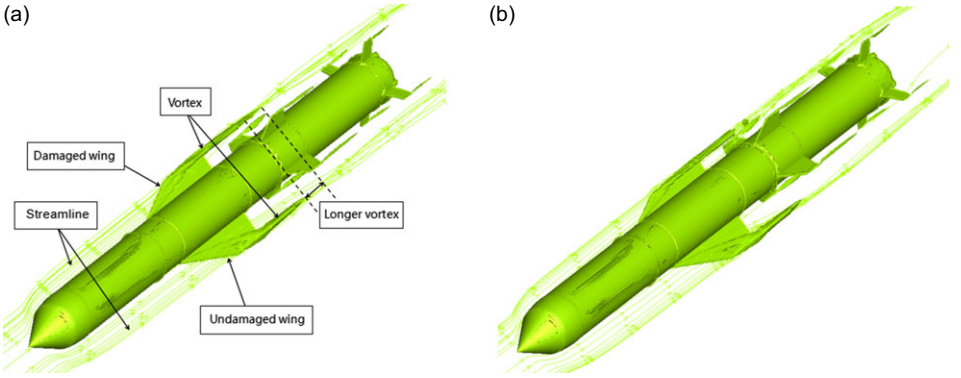

h/l=0.3 damaged model *h/l*=0.5 damaged model

Figure 9. *Streamlines and vortices at* $\alpha = 4°$.

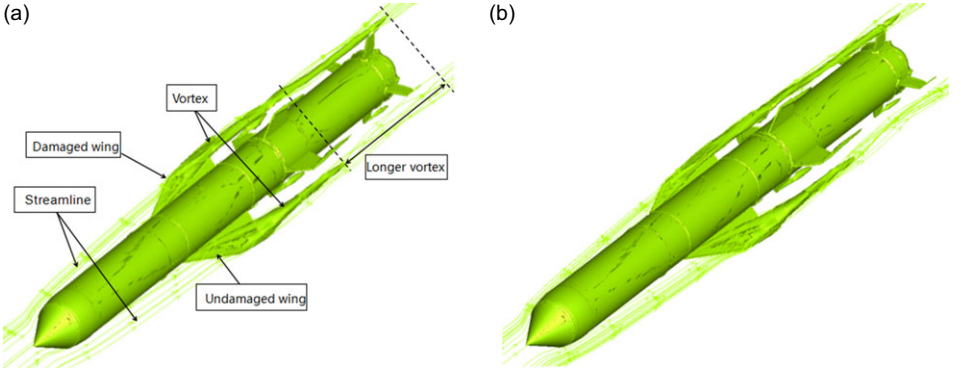

h/l=0.3 damaged model *h/l*=0.5 damaged model

Figure 10. *Streamlines and vortices at* $\alpha = 8°$.

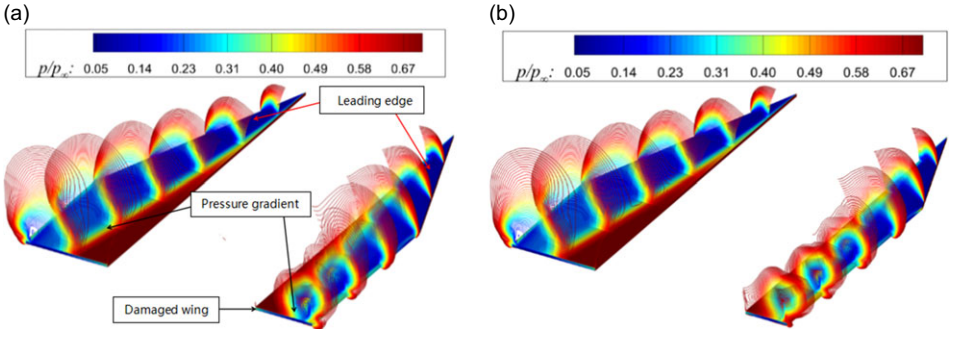

h/l=0.3 damaged model *h/l*=0.5 damaged model

Figure 11. *Pressure contour around wings at* $\alpha = 8°$.

https://doi.org/10.1017/aer.2024.52 Published online by Cambridge University Press

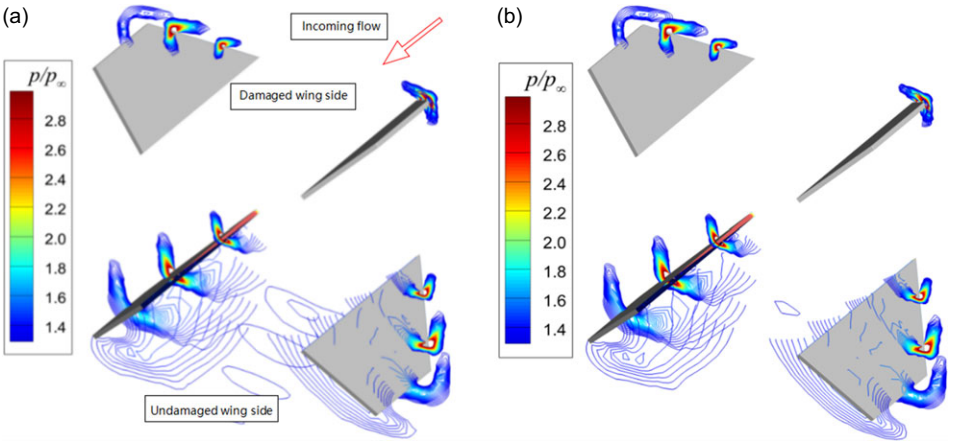

h/l=0.3 damaged model *h/l*=0.5 damaged model

Figure 12. *Pressure contour around rudders at* $\alpha = 8°$.

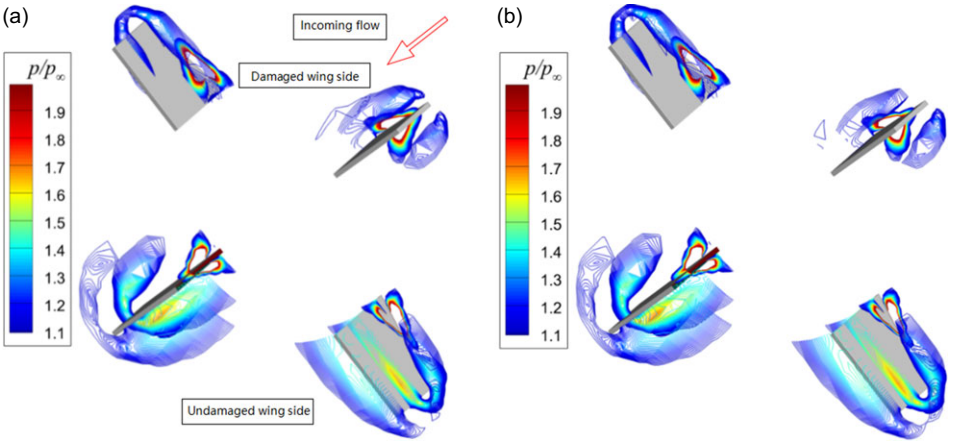

h/l=0.3 damaged model *h/l*=0.5 damaged model

Figure 13. *Pressure contour around fins at* $\alpha = 8°$.

relationship with the damage extent at the same AoA. The wingtip vortices effect of damaged models is weakened, leading to reduction in lift force along with a reduction in lift-induced drag force.

Figures 12 and 13 show that the damaged wing also affects the flow field around the rudders and fins at the rear of the body. Due to the partial loss of right wing, the airflow through the right side of the missile body is faster and the pressure is lower, and a local low pressure region is formed between the upper and lower rudders and fins on the right side. The pressure distribution on the right rudders and fins, especially on the right upper rudder and the fin surface, produces more obvious changes, this is, the pressure distribution on the upper and lower surfaces is not symmetrical. The increased damage extent also has a great influence on the flow field around the rudder and fin at the right upper position. As a result, a counterclockwise roll moment is generated by the rudders and fins of the missile, respectively, to counteract the clockwise roll moment that occurs due to the partial missing of the right wing.

Figure 14 shows the static aerodynamic force and moment coefficient. Compared to the undamaged model, both the drag and lift coefficient of the damaged model are smaller due to the loss of both windward and lift surfaces. With the increase of damage extent, both C_d and C_l are sensitive to the change

https://doi.org/10.1017/aer.2024.52 Published online by Cambridge University Press

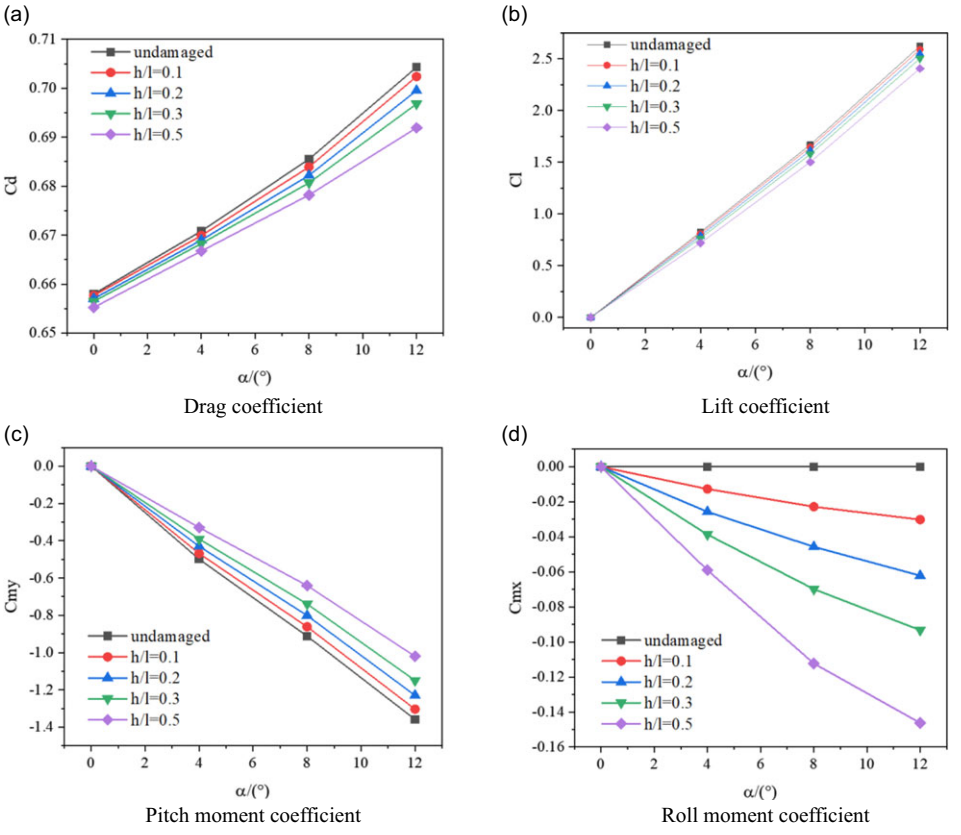

Figure 14. *Static aerodynamic forces and moments.*

with AoA. The rate of change is listed in Tables 5 and 6. The change rate of the drag coefficient increases with increasing damage extent as well as with increasing AoA, while the change rate of the lift coefficient increases with increasing damage extent and decreases with increasing AoA. Meanwhile, Table 6 also shows the nonlinear relationship between the reduction of lift coefficient and the damaged extent at the same AoA.

The pitch moment C_{my} of the missile is negative, which indicates that it can restrain the pitch motion and the missile is statically stable. The figure shows that as the AoA increases, the pitch moment values of several damaged models still basically obey linear changes. The more the missile wing is damaged, the larger the static pitch moment is, but the absolute value is decreasing, and the suppression of pitch motion decreases. That is, the static stability of the missile becomes worse. Due to the front of the missile wing is triangular, the surface area decreases more behind the MRP than in the front when the missile loses partial right wing.

The roll moment C_{mx} of the undamaged model is nearly 0 at all the angles of attack. As the area loss on the right wing increases, the absolute value of the roll moment increases and gradually changes from linear to non-nonlinear. This is due to the missing lifting surface area of the missile's right wing is not linearly related to the missing wingspan.

4.2 Dynamic aerodynamic characteristics

Based on the static solutions, dynamic grid method is used to simulate unsteady small amplitude forced vibration to calculate dynamic aerodynamic parameters. The pitch motion is defined as

https://doi.org/10.1017/aer.2024.52 Published online by Cambridge University Press

Table 5. *C_d change at different AoA*

Extent	$\alpha = 0°$	$\alpha = 4°$	$\alpha = 8°$	$\alpha = 12°$
$h/l = 0.1$	0.109%	0.137%	0.233%	0.267%
$h/l = 0.2$	0.207%	0.274%	0.484%	0.676%
$h/l = 0.3$	0.292%	0.382%	0.710%	1.062%
$h/l = 0.5$	0.480%	0.608%	0.834%	1.755%

Table 6. *C_l change at different AoA*

Extent	$\alpha = 4°$	$\alpha = 8°$	$\alpha = 12°$
$h/l = 0.1$	1.942%	1.486%	1.266%
$h/l = 0.2$	4.418%	3.332%	2.822%
$h/l = 0.3$	7.150%	5.523%	4.592%
$h/l = 0.5$	12.767%	10.067%	8.253%

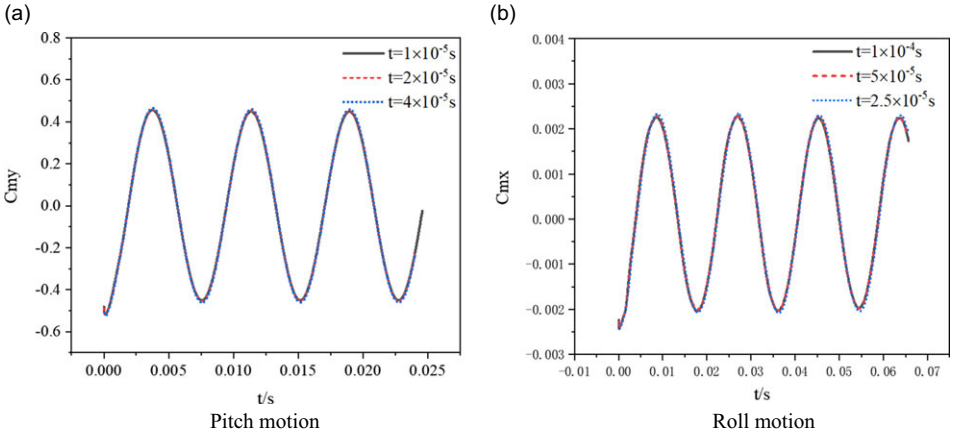

Figure 15. *Validation of moment coefficient with time during pith/roll motion (time step independence validation).*

$\alpha = \theta_0 + \theta_m \sin(\omega t) = \theta_0 + 0.25° \sin(823.2t)$, and the corresponding reduced frequency is $k = \omega l/2V_\infty = 0.24$. The roll motion is defined as $\alpha = \theta_0 + \theta_m \sin(\omega t) = \theta_0 + 0.25° \sin(343t)$, and the corresponding k is 0.1. Other parameters are the same as those in the static calculation.

Due to the unsteady flow involved, the independence of the time step must be validated before the dynamic characteristics calculation. The time step $t_y = 1\times10^{-5}$s, 2×10^{-5}s and 4×10^{-5}s are used to calculate the pitch moment coefficient of the undamaged model at $\alpha = 0°$. And the time step $t_x = 1\times10^{-4}$s, 5×10^{-5}s and 2.5×10^{-5}s are used to calculate the roll moment coefficient of the undamaged model at $\alpha = 0°$. The results in the Fig. 15 show that there is almost no difference in the calculation results. Considering the calculation time cost and calculation accuracy, the time step for calculating the pitch motion is $t_y = 2\times10^{-5}$s, and the time step for calculating the roll motion is $t_x = 5\times10^{-5}$s in this study.

4.2.1 Pitch dynamic derivative

The hysteresis loops of the pitch moment coefficient are presented in Fig. 16. The hysteresis loops is obviously elliptical in shape, and the angle between its major axis and the x-axis is defined as the azimuth, as shown in Fig. 17. The circumferential direction of all curves is counterclockwise, which indicates the

https://doi.org/10.1017/aer.2024.52 Published online by Cambridge University Press

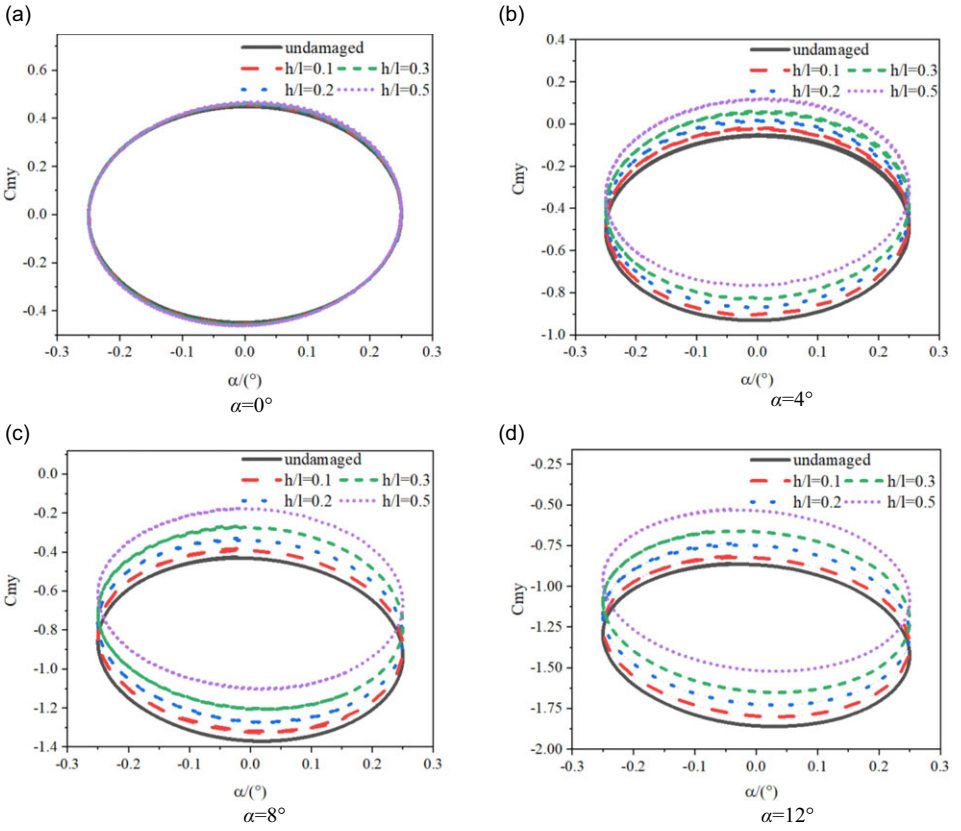

Figure 16. *Hysteresis loops of pitch moment coefficient at different AoA.*

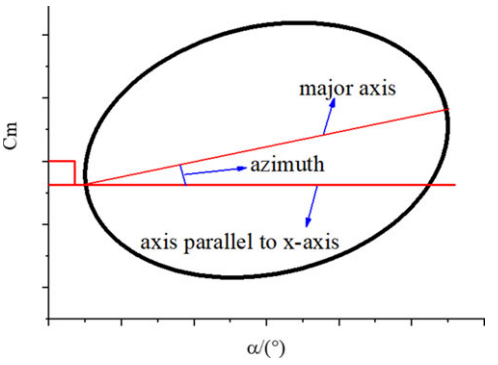

Figure 17. *Diagram of the azimuth.*

missile obtained damping characteristics of pitch moment at all attack angles. Although the different extents of the missing right wing parts, the azimuths and sizes of the hysteresis loops hardly change at the same AoA, only causing different areas of the hysteresis loops: the hysteresis loops area increases slightly with increasing of the damage extent.

Comparing the hysteresis loops at different AoA, the azimuths change. The azimuths of $\alpha = 4^\circ$ are opposite to that of $\alpha = 8^\circ$ and $\alpha = 12^\circ$. Under the condition of the $\alpha = 4^\circ$ and the same absolute value of

https://doi.org/10.1017/aer.2024.52 Published online by Cambridge University Press

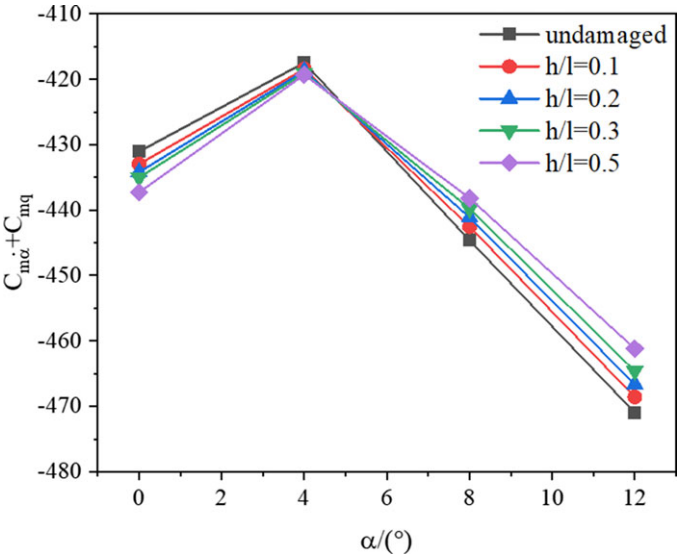

Figure 18. *Combined dynamic derivative of pitch moment.*

oscillation instantaneous AoA, the longitudinal damping value of positive instantaneous AoA is larger than that of the negative instantaneous AoA. On the contrary, the longitudinal damping value at the negative instantaneous AoA is larger than that at the positive instantaneous AoA under the condition of $\alpha = 8°$. The results of $\alpha = 12°$ is the same as that of $\alpha = 8°$.

The pitch combined dynamic derivatives are shown in Fig. 18. With the increase of the AoA, the pitch combined dynamic derivatives $C_{m\dot{\alpha}} + C_{mq}$ of the damaged model and the undamaged models all increase at first and then decrease. This phenomenon is consistent with the changing trend of azimuth with the AoA mentioned earlier. However, the specific change of $C_{m\dot{\alpha}} + C_{mq}$ among individual damage models is different. At $\alpha = 0°$, the values of $C_{m\dot{\alpha}} + C_{mq}$ decrease with the increase of damage extent. At $\alpha = 4°$, the values of $C_{m\dot{\alpha}} + C_{mq}$ are basically the same for different damage extent. When AoA is $\alpha = 8°$, the $C_{m\dot{\alpha}} + C_{mq}$ of the damaged model becomes larger than that of the undamaged model, and this phenomenon is more obvious at $\alpha = 12°$. The combined dynamic derivative calculation indicates that the differences among damaged and undamaged models are mainly caused by the different missing areas of effective lifting surface before and after the moment reference point.

With the increase of AoA, the absolute values of the pitch combined dynamic derivatives first increases and then decreases with the increase of damage extent, which indicates the pitch damping characteristics don't get worse in all cases, even slightly increase at small AoA. For the missile in this study, the dynamic performance is the worst at $\alpha = 4°$. Compared with the undamaged model, the dynamic performance of the damaged models is even better when the AoA is within 5°. However, when the AoA exceeds 5°, it becomes worse rapidly. Generally speaking, at small angles of attack, the damage to one side of wing has little effect on the pitch dynamic performance of the missile.

4.2.2 Roll dynamic derivative

The hysteresis loops of the roll moment coefficient are presented in Fig. 19. After the wings being damaged, the hysteresis loop areas of their roll moment coefficients decrease, and the greater the damage extent, the smaller the hysteresis loops area, which is obvious at $\alpha = 0°$. Different from the pitch direction, damage causes a great influence on the dynamic performances in the roll direction. The roll combined dynamic derivatives $C_{mx\dot{\alpha}} + C_{mxq}$ of several models at different AoA are shown in Fig. 20. For all models, the absolute values of the roll combined dynamic derivatives first decrease and then increase

https://doi.org/10.1017/aer.2024.52 Published online by Cambridge University Press

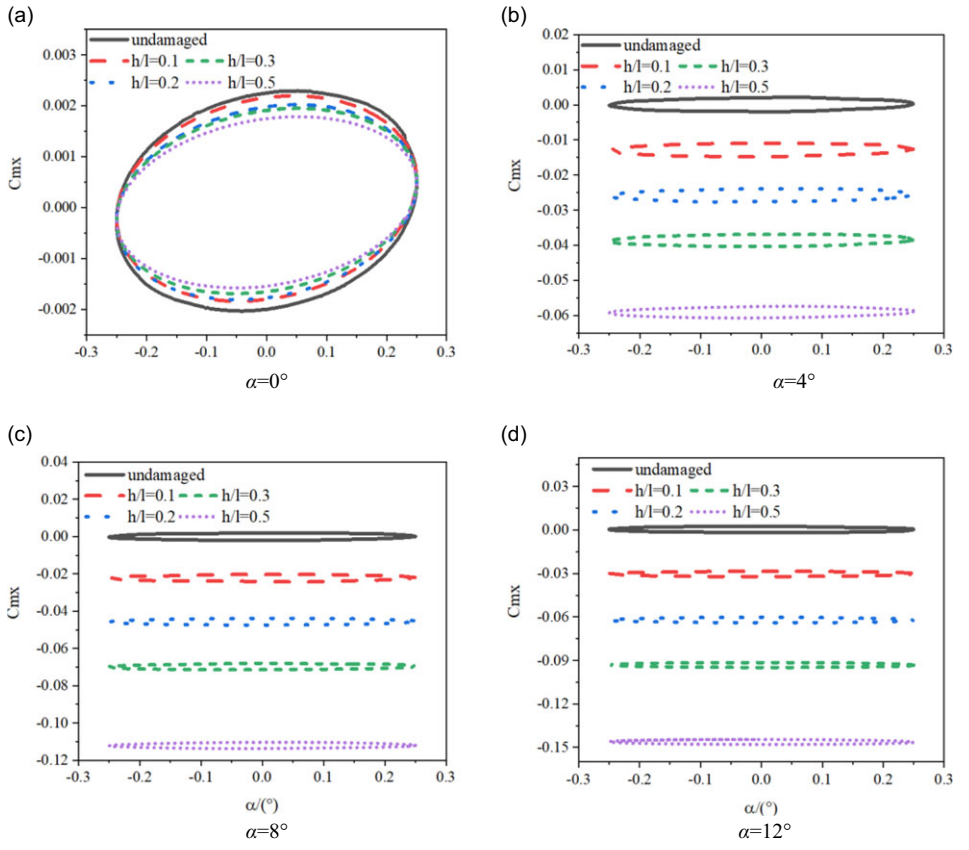

Figure 19. *Hysteresis loops of roll moment coefficient at different AoA.*

with the increase of the AoA. Compared to the undamaged model, the values of dynamic derivative of damaged models decrease a lot. When the damage is 0.5l, the absolute value of roll combined dynamic derivative decreases even more than 20%. Considering that the missile has X-shaped rudders and fins, this value is quite large. And the absolute value of the roll combined dynamic derivatives first decreases and then increases with the increase of the AoA, and this trend is the same as that of pitch combined dynamic derivatives. The turning point appears between $\alpha = 4°$ and $\alpha = 8°$. According to Fig. 18, it is guessed that it may appear around $\alpha = 5°$. However, different from the pitch direction, the roll performance of damaged models deteriorates at all angles of attack, which is also consistent with reality.

4.2.3 Pitch-roll coupling dynamic derivative

The unsteady roll moment coefficient is shown in Fig. 21. The pitch-roll coupling moment caused by pitch oscillation is in the same order of magnitude as the roll moment, so it cannot be neglected. At $\alpha = 0°$, the pitch-roll moments of all models differ by several orders of magnitude from other angles of attack, and it is nearly 0, so the hysteresis loop is not shown. When AoA is more than 0°, the force on the left and right sides of the missile is unbalanced in pitch oscillation, which in turn leads to roll moment. Meanwhile, the pressure centre is away from the centre of gravity in the longitudinal and transverse directions respectively. It leads to an increase in the areas of the hysteresis loops, which makes the dynamic coupling characteristics between the pitch and roll directions increasing apparently. With the

https://doi.org/10.1017/aer.2024.52 Published online by Cambridge University Press

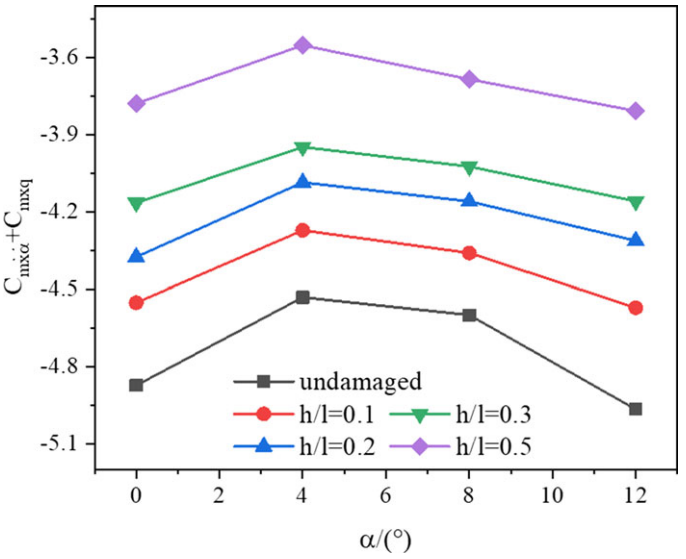

Figure 20. *Combined dynamic derivative of roll moment.*

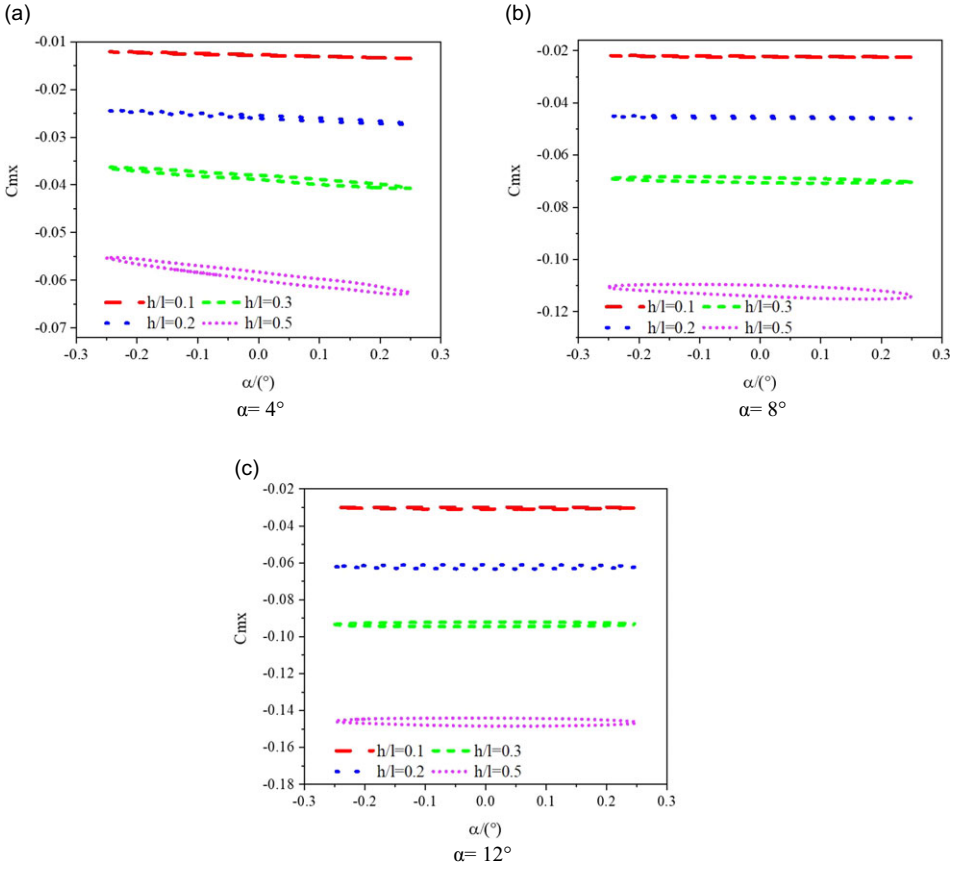

Figure 21. *Unsteady roll moment coefficient caused by the pitch oscillation.*

https://doi.org/10.1017/aer.2024.52 Published online by Cambridge University Press

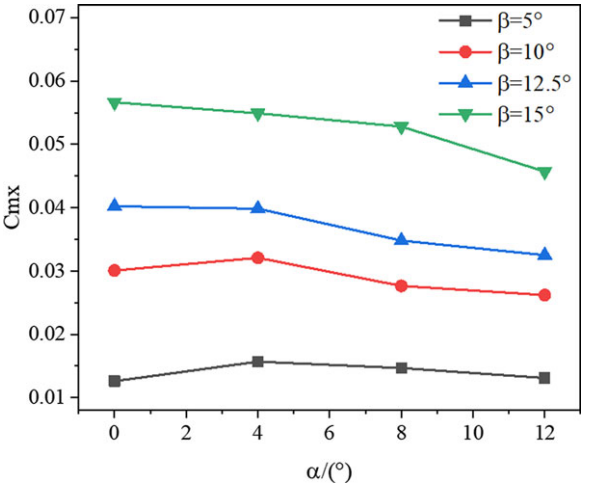

Figure 22. *Roll moment coefficient caused by one rudder deflection.*

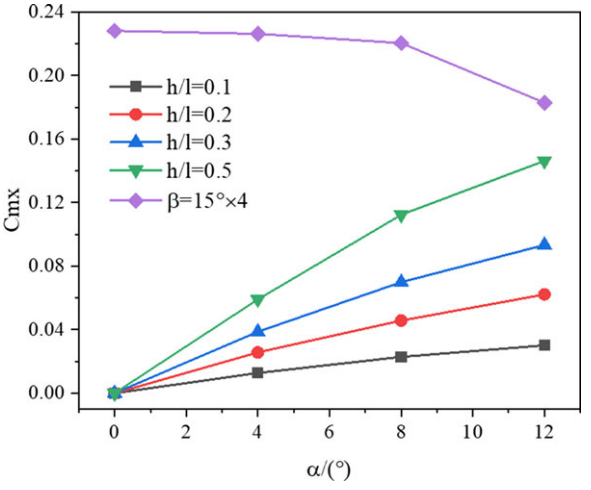

Figure 23. *The static roll moments provided by four rudders, and the roll moments required of different damaged models.*

increase of the initial AoA, the azimuths of hysteresis loops also decrease, and the pitch-roll hysteresis loops tend to be horizontal when the instantaneous AoA changes.

4.3 Damage limit of missile wing

After the unilateral wing of the missile is damaged, roll dispersion results from lift non-averaging produced by body-fixed vehicle asymmetries will appear [38, 39]. Some aerodynamic performances can be saved by controlling the deflection of the rudders. The damage limit of the missile wing is judged since the missile does not roll. That is, the static balance of the missile after the wing damage is maintained by four rudder deflections. The full roll moment of the missile can be expressed as:

$$C_m = C_{m_0} + C_m(\alpha) \cdot \alpha + C_m(\beta) \cdot \beta \tag{8}$$

https://doi.org/10.1017/aer.2024.52 Published online by Cambridge University Press

Table 7. *Trim validation of the $h/l = 0.625$ damaged model at $\alpha = 12°$*

C_{mxr}	C_{mxt}	C_{mxt}/C_{mxr}
−0.1829	0.0037	−2.023%

where, C_m is the full roll moment, C_{m0} is the zero-liter moment, $C_m(\alpha)\cdot\alpha$ is the roll moment caused by the AoA α, and $C_m(\beta)\cdot\beta$ is the trim moment caused by the rudder deflection angle β.

Figure 22 shows the roll moment provided by one rudder at different deflection angles. In the figure, β represents the deflection angle of a single rudder. It can be seen from the figure that with the increase of the AoA, the static roll moment provided by the smaller rudder deflection angles first increase and then decrease. The roll moments provided by the larger rudder deflection angles decrease continuously.

The deflection efficiency of the remaining three rudders is regarded as the superposition of one rudder. Through this simplified processing, the roll moment provided by the four rudders at different angles of attack can be obtained. The maximum deflection angle of each rudder is limited to 15°. Figure 23 shows the static roll moments that can be provided when all four rudders are deflected to 15°, as well as the roll moment required to maintain balance for four models with different extents of damage at different angles of attack.

As can be seen in Fig. 23, even at a maximum angle-of-attack of $\alpha = 12°$, all damaged models in this study can achieve roll moment balancing. Next, the damage limit of missile wing at $\alpha = 12°$ will be studied, which is the worst flight condition. According to the relationship between the change of roll moment coefficient and the damage extent of missile wing, it is found that it basically conforms to the linear change law: $C_{mx} = -0.2941(h/l)$. When the four rudders are all deflected to 15°, the maximum roll moment available is $C_{mxr} = -0.1829$. Then, the maximum allowable wing damage extent is $h/l = 0.625$ when the missile does not roll.

Finally, the correctness of the damage limit needs to be validated by numerical simulation. The results are shown in Table 7. C_{mxt} represents the roll moment coefficient of the missile with right wing $h/l = 0.625$ damage trimmed by rudders deflection. The relative error C_{mxt}/C_{mxr} is −2.023%. This is a relatively small value. This shows that the limit damage extent of missile wing is $h/l = 0.625$ with high credibility.

5.0 Conclusions

CFD simulation are implemented on the simplified model of supersonic cruise missile, including undamaged model and four models with different damage extents of wing. The static aerodynamic force and moment of all models have been calculated and compared. On this basis, the dynamic pitch, roll and pitch-roll coupling moments are further computed. The combined dynamic derivatives are obtained and their variation rules after being damaged are found. The main conclusions are as follows:

(1) The partial missing area of the lift surface on the right wing causes geometric asymmetry, which further leads to the asymmetry of the flow field. Compared to the undamaged model, the damaged models have small drag and lift coefficients. With the increase of damage extent, both drag and lift coefficients are sensitive to the change of the AoA, but their respective rates of change are different: the change rate of drag coefficient at the larger AoA is greater than that at the smaller AoA. On the contrary, the change rate of lift coefficient at the larger AoA is smaller than that at the lower AoA. Meanwhile, the absolute value of static pitch moment decreases, and the suppression of missile pitch motion weakens. The absolute value of the roll moment increases, and gradually changes from linear to non-nonlinear.

(2) The dynamic pitch and roll performances of the missile are both the worst when the AoA is $\alpha = 4°$. Compared with the undamaged model, the pitch performance of the damaged models is even better when the AoA is within 5°, but it becomes worse when the AoA exceeds 5°. For all models, the absolute values of the roll combined dynamic derivatives first decrease and then increase with the increase of the AoA

https://doi.org/10.1017/aer.2024.52 Published online by Cambridge University Press

like the tendency of the pitch direction. The turning point appears around $\alpha = 5°$. Different from the pitch direction, the roll performance of damaged models deteriorates at all angles of attack. Relatively speaking, the influence of wing damage on the roll direction is much greater than that on the pitch direction. In addition, the extension in the loss area causes the dynamic coupling characteristic between the pitch and roll directions to increase apparently.

(3) The maximum allowable damage extent of the missile wing that can achieve static trim is obtained at $\alpha = 12°$ and the maximum deflection angle of the single rudder is 15°.When the four rudders are all deflected to 15°, the allowable damage limit of the missile wing that maintains the balance of the roll direction is $h/l = 0.625$. And its credibility is proved by numerical validation.

Acknowledgements. The authors would like to acknowledge the support of National Natural Science Foundation of China (Grant No. 11602109).

Competing interests. The authors declare that they have no competing interests.

References

[1] Trisolini, M., Lewis, H.G. and Colombo, C. Spacecraft design optimization for demise and survivability, *Aerosp. Sci. Technol.*, 2018, **77**, pp 638–657.
[2] Zhang, J., Yang, X.K. and Yang, L.Y. Virtual-command-based model reference adaptive control for abrupt structurally damaged aircraft, *Aerosp. Sci. Technol.*, 2018, **78**, (1), pp 452–460.
[3] An, X.B., Qi, Z.H., Ji, Y.W. and Lin, H.S. The strategy of collision avoidance between missile and space debris based on genetic algorithm, 2016 International Conference on Information System and Artificial Intelligence (ISAI), 2016.
[4] Kim, S., Lee, Y. and Tahk, M. New structure for an aerodynamic fin control system for tail fin-controlled STT Missiles. *J. Aerospace Eng.*, 2011, **24**, (4), pp 505–510.
[5] Cao Y.J., Cao, Z.Q., Zuo, Y.J., Huo, L.B., Qiu, J.P. and Zuo, D.Q. Numerical and experimental investigation of fitting tolerance effects on damage and failure of CFRP/Ti double-lap single-bolt joints, *Aerosp. Sci. Technol.*, 2018, **78**, (1), pp 461–470.
[6] Arif, I., Ansari, T. and Javed, A. Aircraft stability characteristics in a single horizontal tail failure and evaluation of countermeasures for safe landing, *J. Appl. Fluid Mech.*, 2021, **14**, (3), pp 847–859.
[7] Elkarim, Y. and Elrahman, M. A review on methods used for estimation of aerodynamic of damaged aircraft, *Int. J. Res. Aeronaut. Mech. Eng.*, 2015, **3**, pp 7–21.
[8] Harris, J. and Slegers, N. Performance of a fire-and-forget anti-tank missile with a damaged wing, *Math. Comput. Model.*, 2009, **50**, (1-2), pp 292–305.
[9] Irwin, A.J. and Render, P. The influence of internal structure on the aerodynamic characteristics of battle-damaged wings, 14th Applied Aerodynamics Conference, 1996.
[10] Djellal, S. and Ouibrahim, A. Aerodynamic performances of battle-damaged and repaired wings of an aircraft model, *J. Aircraft*, 2008, **45**, (6), pp 2009–2023.
[11] Wen, Y., Yang, L.Y. and Shen, G.Z. Aerodynamic characteristics analysis and capability assessment of structural damaged aircraft with advanced configuration, 2011 International Conference on Electronics, Communications and Control, 2011.
[12] Etemadi, F., Etemadi, M., Mani, M. and Pooladsanj, S. Experimental and numerical analysis of aerodynamic effects of repair patches on damaged airfoils, *J. Mech. Sci. Technol.*, 2017, **31**, (2), pp 651–658.
[13] Zkaya, Z. and Kayran, A. Nonlinear static aeroelastic behavior of composite missile fin with interlaminar and intralaminar damage, 2018 AIAA/ASCE/AHS/ASC Structures, Structural Dynamics, and Materials Conference, 2018.
[14] Yang, Z.Y., Samad-Suhaeb, M. and Render, P. Computational study of a battle damaged finite aspect ratio wing, 30th AIAA Applied Aerodynamics Conference, 2012.
[15] Shankar, P. Characterization of aircraft trim points using continuation methods and bifurcation analysis, AIAA Guidance, Navigation and Control (GNC) Conference, 2013.
[16] Elgersma, M.R. and Morton, B.G. Nonlinear six-degree-of-freedom aircraft trim, *J. Guid. Control and Dynam.*, 2000, **23**, (2), pp 305–311.
[17] Shah, G. Aerodynamic effects and modeling of damage to transport aircraft, AIAA Atmospheric Flight Mechanics Conference and Exhibit, 2008.
[18] Mikhail, A.G. Fin damage and mass offset for kinetic energy projectile spin/pitch lock-in, *J. Spacecraft Rockets*, 1998, **35**, (3), pp 287–295.
[19] Mi, B.G. Simulation on the dynamic stability derivatives of battle-structure-damaged aircrafts, *Def. Technol.*, 2021, **17**, (3), pp 987–1001.
[20] Lanham, D. Design and qualification report for the javelin launch tube ruggedization program Navel surface warfare center, NSWCCR/RDTR-07/27, Crane, IN, 2007.
[21] Struchkov, A.V., Kozelkov, A.S., Volkov, K.N., Kurkin, A.A., Zhuckov, R.N. and Sarazov, A.V. Numerical simulation of aerodynamic problems based on adaptive mesh refinement method, *Acta Astronaut.*, 2020, **172**, pp 7–15.

https://doi.org/10.1017/aer.2024.52 Published online by Cambridge University Press

[22] Sumnu, A. and Güzelbey, I.H. CFD simulations and external shape optimization of missile with wing and tailfin configuration to improve aerodynamic performance, *J. Appl. Fluid Mech.*, 2021, **14**, (6), pp 1795–1807.
[23] Elisov, N.A., Ishkov, S.A. and Shakhov, V.G. Numerical analysis of air dissociation influence on spaceplane aerodynamic characteristics, *Acta Astronaut.*, 2018, **148**, pp 153–162.
[24] Yang, L.Z., Wang, M.H. and Gao, Z.H. Numerical investigation of unsteady aerodynamic characteristics of a pitching missile, *Chin. J. Appl. Mech.*, 2009, **15**, (2), pp 129–136.
[25] Spalart, P.R. and Allmaras, S.R. A one-equation turbulence model for aerodynamic flows, *Rech. Aerospatiale*, 1994, **1**, pp 5–21.
[26] Meng, Y.S., Yan, L., Huang, W. and Tong, X.Y. Numerical investigation of the aerodynamic characteristics of a missile, *IOP Conf. Ser. Mater. Sci. Eng.*, 2020, **887**, (1), p 012001.
[27] Render, P.M., Samaad-Suhaeb, M., Yang, Z.Y. and Mani, M. Aerodynamics of battle-damaged finite-aspect-ratio wings, *J. Aircraft*, 2009, **46**, (3), pp 997–1004.
[28] Jinbum, H. and Seungsoo, L. Numerical study on lateral jet interaction in supersonic crossflows, *Aerosp. Sci. Technol.*, 2018, **80**, pp 315–328.
[29] Spalart, P.R. and Allmaras, S.R. A one-equation turbulence model for aerodynamic flows, 30th Aerospace Sciences Meeting and Exhibit, 1992.
[30] Allen, J. and Ghoreyshi, M. Forced motions design for aerodynamic identification and modeling of a generic missile configuration, *Aerosp. Sci. Technol.*, 2018, **77**, pp 742–754.
[31] Wu, Z.L., Lv, B.Y. and Cao, Y.H. Heavy rain effects on aircraft lateral/directional stability and control determined from numerical simulation data, *Aerosp. Sci. Technol.*, 2018, **80**, pp 472–481.
[32] Oktay, E. and Akay, H. CFD predictions of dynamic derivatives for missiles, 40th AIAA Aerospace Sciences Meeting and Exhibit, 2002.
[33] Bhagwandin, V.A. and Sahu, J. Numerical prediction of pitch damping stability derivatives for finned projectiles, *J. Spacecraft Rockets*, 2014, **51**, (5), pp 1603–1618.
[34] Mi, B.G. Computational investigation of simulation on the dynamic derivatives of flight vehicle, *Acta Aerodyn. Sinica*, 2014, **32**, (6), pp 834–838.
[35] Dupuis, A.D. and Hathaway, W. Aeroballistic range tests of the basic finner reference projectile at supersonic velocities, Defence Research Establishment Valcartier (QUEBEC), 1997.
[36] Dupuis A.D. Aeroballistic range and wind tunnel tests of the basic finner reference projectile from subsonic to high supersonic velocities, Defense Research and Development Canada Valcartier Canada TM, 2002.
[37] Green, L., Spence, A. and Murphy, P. Computational methods for dynamic stability and control derivatives, 42nd AIAA Aerospace Sciences Meeting and Exhibit, 2004.
[38] Fuess B.F. Impact dispersion due to mass and aerodynamic asymmetries, *J. Spacecraft Rockets*, 1967, **4**, (10), pp 1402–1403.
[39] Crenshaw, J.P. (1971). Effect of lift with roll rate variation on re-entry vehicle impact, *J. Spacecraft Rockets*, 1971, **8**, (5), pp 483–488.

Cite this article: Zhuo C.F., He Z.R., Ren X.B. and Wang Y.K. (2024). Static and dynamic characteristics of supersonic cruise missile with damaged wing. *The Aeronautical Journal*, **128**, 2634–2655. https://doi.org/10.1017/aer.2024.52